2.2.5 Water Chemistry Data

Though not literally a parameter used for the numerical modeling, the chemical data from groundwater samples at Amchitka are used for assessing the model calibration. The data are presented in Table 1.2, with a discussion of the salinity profiles for the three locations.

Collection of representative groundwater samples from deep wells during drilling programs is very challenging. Samples from discrete depth intervals were generally collected by swabbing water from a zone isolated by packers. Pumped samples were also collected, but tended to be from very long intervals in the boreholes. The primary problem is the purging of drilling fluids and fluids from zones other than the one being isolated. Significant differences existed in the construction of UAe-1 and UAe-2, and are described in detail by Fenske (1972). UAe-1 was drilled with a water-based mud using normal circulation. UAe-2 was drilled with water using a reverse circulation method that limits pressure against the formation and consequent fluid loss. Drilling and testing of UAe-2 required 105 days, whereas considerable difficulties were encountered in both the drilling and testing of UAe-1, which required 142 days to complete. Fenske notes that the scatter in the UAe-1 chemical data below about 1,400 m below mean sea level suggests contamination. The Long Shot holes were all drilled using a bentonite mud comparable to that used in oil-field operations (U.S. Army Corps of Engineers and USGS, 1965). It is noted that the drilling mud in the hole (left in due to caving problems) and the mud forced into the formation restricted the flow of formation water. "Clear water" was never swabbed from EH-5, leading the workers to conclude that all of the samples collected contained mud.

Given the drilling histories and pH values of the groundwater samples, the chemical data from UAe-2 are considered to have the highest quality. Water chemistry data from Cannikin and Long Shot contain more uncertainty and are less likely to be representative of in-situ conditions. In addition to the question of the degree of representativeness of the water samples of in-situ conditions, the use of the chemical data for calibration is subject to uncertainty introduced by transient flow processes. Dispersion resulting from short period fluctuations due to tidal and barometric effects can be approximated by adjusting the dispersion term during calibration. However, if there is a significant lag in the response of the chemical system to fluctuations in the transition zone brought about by climate change, the transition zone midpoint and spreading may not coincide with those that would be at equilibrium with the hydraulically defined transition zone. Given that the last major sea level change was in a negative direction (lower sea level due to glaciation), this may have left a deeper freshwater lens relict of the lower sea level condition than would be in equilibrium with the current head configuration.

2.3 Numerical Modeling Strategy

Based on previous experience with large-scale flow and radioactive transport modeling, a deterministic approach for flow and transport analyses is not considered to be sufficient for the Amchitka sites. With limited data to support the choice for each individual parameter, the deterministic approach is inadequate in describing the uncertainty of the processes involved. Therefore, a multi-parameter stochastic modeling approach is used, through which the uncertainty

in the model conceptualization and the flow and transport parameters can be addressed to a certain degree of satisfaction.

The approach used here acknowledges the uncertainty in the parameters and includes it in the analysis. This allows the contaminant breakthrough curves to contain this uncertainty, expressed as a standard deviation around a mean value. Including uncertainty from the flow and transport parameters has been found to be critical to risk assessments, as this source of uncertainty is often quite large and contributes significantly to overall uncertainty in risk (Andricevic et al., 1994; Andricevic and Cvetkovic, 1996). Whether the degree of parametric uncertainty is acceptable or not for the objective of conducting a human-health-risk assessment for Amchitka can be determined from the results of the risk assessment.

The modeling of the island's nuclear tests encompasses two major processes: 1) the flow modeling, which includes density-driven flow, saltwater intrusion, and heat-driven flow, and 2) the transport modeling, which combines radioactive transport and decay, retardation processes, source term and glass dissolution, and matrix diffusion. Modeling each of the two processes is fraught with many uncertainties and difficulties determining the values of the parameters governing these processes. The final modeling approach and results should, therefore, reflect the best of our ability to overcome these difficulties and address these uncertainties. The conceptual model and the modeling strategy that are used to evaluate and address the many uncertainties associated with this analysis are presented in the following sections.

2.3.1 Modeling Approach

The modeling approach begins with the flow problem that is coupled with saltwater intrusion and heat effects. One can list the main uncertain parameters that influence the solution of the flow problem for the velocity field. The list includes, but may not be limited to, recharge, hydraulic conductivity, macrodispersivity affecting saltwater dispersion, heat parameters, the island half-width, etc. The impact of any of these parameters is either to change the depth to the freshwater-saltwater interface or transition zone, or to change the width of the transition zone. In either case, the velocity pattern changes significantly, which consequently influences the radionuclide migration from the cavity toward the sea. It is well known (Pohll et al., 1999; Pohlmann et al., 1999) that the most influential parameters are those changing the travel time of the radionuclides from the cavity to the seepage face across the sea floor. However, due to the complexity of the processes involved, it may be difficult to pre-determine those parameters for reducing the above list.

For the transport of radionuclides, many processes have to be considered. Hydraulic versus geochemical release, advection and macrodispersion dictated by the heterogeneous velocity field, local-scale dispersion, matrix diffusion, retardation and decay are important processes that encounter a large number of uncertainties. The uncertain parameters here include effective porosity, glass dissolution rate, retardation factor, local dispersivity, and matrix diffusion coefficient. Only effective porosity and retardation change the travel time; the other factors cause plume spreading, tailing effects and reduction of mass fluxes and concentrations. Again, these parameters are

computed or assumed with large uncertainties and as such it is important to address the effect of the uncertainty in each parameter on the transport results.

The approach used here is of a stochastic nature and represents an attempt to evaluate the effect of input uncertainties on the associated uncertainties of the output. Since the solution to obtain the velocity field encounters a simultaneous solution to the flow and the advection-dispersion equation, some of the parameters governing transport processes are considered when solving the flow problem. This includes the effective porosity and the macrodispersivity values used for the saltwater intrusion problem.

Consider the four uncertain parameters of the flow model, conductivity, recharge, fracture porosity and macrodispersivity. Based on available data, calibration results, and results of previous studies of Amchitka, a best estimate (mean) for each parameter and an associated degree of uncertainty can be hypothesized. For example, the available hydraulic conductivity data can be analyzed and tied to the calibration results to yield a best estimate (mean value) for a spatially uniform (homogeneous) conductivity and the uncertainty of the estimate. For other parameters, such as macrodispersivity, the mean value can be obtained in the calibration process where an attempt is made to match the measured concentration and/or head values. A certain degree of parameter uncertainty can then be added to the macrodispersivity mean value. For each parameter, a distribution of random values above and below the mean can be generated using the mean and the uncertainty range estimated from data or calibration.

The selection of the parameter distributions is dictated by a number of factors. If data are available, the distribution of a particular parameter should produce the range of values that is indicated by the data. Calibration results set certain limits to the tails of the distribution of some parameters, such as recharge and hydraulic conductivity. Also, when a parameter range covers orders of magnitude, distributions such as uniform or normal are difficult to use for producing this variability range, and a lognormal distribution works better in such cases. In some cases, a normal or a lognormal distribution is used to generate parameter values but the tails of the distribution are truncated to remove the extreme values that are in violation of certain aspects and assumptions of the model.

The first stage of the modeling then becomes the evaluation of the effect of each uncertain parameter on the transport results. Random values of any parameter can be sampled from a hypothetical distribution to form an ensemble of N values with $N = 100$ in all cases of the first stage. While fixing all other flow and transport parameters at their mean (best estimate) values, Monte Carlo simulations are performed for flow coupled with saltwater intrusion and radioactive transport coupled with matrix diffusion. By analyzing the ensemble of the resulting plumes, a direct correlation between the parameter uncertainty and that of the results can be established. This procedure is repeated for all the uncertain parameters in the flow and transport lists. This approach seems computationally demanding and time consuming. However, only flow parameters require generating multiple flow realizations. The effect of the uncertainties in transport parameters will be addressed using a single flow realization and multiple transport solutions using the random values of the studied parameter. This realization is selected based on setting all flow and other transport

parameters to their mean values. The final objective of this first step is to filter out those parameters whose uncertainties have minor effects on the transport results. Another objective is to quantitatively address the effect of the uncertainty of each individual parameter without any overlap with other uncertainties. It should be mentioned here that the first modeling stage is only performed for Milrow. When the list of uncertain parameters is selected for the second modeling stage at Milrow, the same list of parameters will be employed in modeling Cannikin and Long Shot.

Once the set of important parameters is determined, a new set of Monte Carlo simulations is designed for the second stage. The flow set will be generated using values for the influential, uncertain parameters drawn at random from their distributions. That is, for realization i, all the values of the flow parameters in the reduced list will be randomly generated based on the distributions used in the first step or new distributions. The new set of M flow realizations, with M between 200 and 300, will be used for the transport simulation such that for realization i, each transport parameter in the reduced list (if any) will be selected randomly from its distribution. In this way, all different combinations between flow and transport parameters can be encountered. For example, a case with a very high conductivity, a very low porosity and weak retardation is as likely to be generated as a case with very low conductivity, very high porosity and strong retardation. The set of M transport results will be statistically analyzed for each individual radionuclide to obtain expected mass fluxes, concentrations, and seepage-face location, as well as the associated uncertainties.

The second modeling stage described above will be performed for the three underground nuclear tests. One of the important advantages of the proposed approach is the fact that the first step will give an idea about which parameter uncertainty should be reduced the most to significantly reduce the uncertainty of the results. This will help as a guide in the event that fieldwork is required to collect more data. The important issue to remember here is that the results will be dependent on the initial choice of mean and range for different parameters. Since these mean values themselves encounter large uncertainties as will be seen in the calibration discussion, the results are largely dependent on this choice.

2.3.2 Code Selection

A large number of codes are available that can simulate one or more of the processes that have been identified as potentially important to radionuclide transport beneath Amchitka Island. Many of the codes are optimally designed for specific portions of the problem, or have enhanced capabilities that are attractive for some portions of the proposed work. A modeling scheme that will capitalize on the optimal performance of some codes to investigate individual aspects of the flow and transport processes has been devised. Information gained from the subtasks of the modeling effort will be combined into a final conceptual and numerical simulation of the radionuclide transport. For example, the popular USGS code SUTRA is only available in two-dimensions and does not simultaneously solve for heat and solute transport. An alternative selection is FEFLOW, which is available in three-dimensions and can solve heat and mass transport simultaneously. FEFLOW comes with a graphical user interface and an automatic mesh generator for finite-element discretization. Figure 2.6 shows a finite-element mesh generated using FEFLOW. This figure
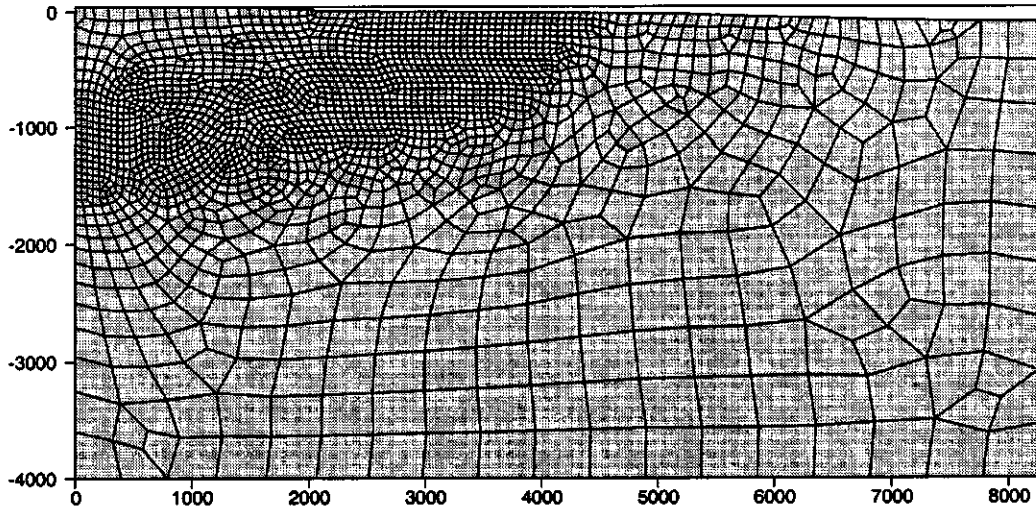
Figure 2.6. A finite-element mesh generated by FEFLOW for the modeled domain showing variable element size with fine resolution at the location of the transition zone.

highlights two points concerning code capability. First, finite-element solutions are vastly more optimized for the seawater intrusion problem because the elements can be made very small throughout the transition zone region without unduly raising the number of elements (and the computational difficulty). Second, the geometry and parameters can be varied almost instantaneously in the graphical user interface (GUI) environment and the results easily compared. For these reasons, the finite-element code FEFLOW is considered the optimal platform for all of the simulations.

The FEFLOW code (Diersch, 1998) is used for the base-case simulations in two dimensions and for addressing issues involving three-dimensional geometry (including the influence on flow patterns of fault zones and rubble chimney configuration) and coupled heat and solute transport (geothermal heat and heat generated by the nuclear explosion). FEFLOW is a finite-element simulation package available from the WASY Institute for Water Resources Planning and Systems Research Ltd. that is developed for two-dimensional and three-dimensional density-dependent flow, mass, and heat transport processes in groundwater, and is generally well-suited for the Amchitka problem.

The groundwater flow problem modeled here requires a description of variable density fluid flow coupled with transport of both salt and heat. The fluid flow is simulated using a form of the Darcy equation generalized for a variable-density fluid. The approach is formulated in terms of the equivalent freshwater head, h_f, and the freshwater hydraulic conductivity, K_f, as

$$h_f = \frac{p}{\rho_0 g} + z \qquad (2.4)$$

and

$$K_f = \frac{\rho_0 g}{\mu} k \qquad (2.5)$$

respectively, where p is fluid pressure, ρ_0 is a reference density of freshwater, g is gravitational acceleration, z is elevation, μ is fluid viscosity, and k is the permeability tensor. K_f is calculated through Equation (2.5) using actual local concentration and temperature effects on density and viscosity implied by the buoyancy term and the viscosity function, given the appropriate reference temperature and concentration for the K measurements. The flow equation can then be written for Darcy flux as

$$q = -K_f \cdot \left(\nabla h_f - \frac{\rho - \rho_0}{\rho_0} \nabla z \right) \qquad (2.6)$$

The density-dependent relations in the coupled transport system employs the extended Boussinesq approximation (Diersch, 1998), where the conservation of fluid mass is described in the generalized form

$$S_s \frac{\partial h}{\partial t} + \nabla \cdot q = Q_\rho + Q_{EB}(C, T) \qquad (2.7)$$

where S_s is the specific storage coefficient (compressibility), Q_ρ is the specific source/sink rate of fluid, and $Q_{EB}(C, T)$ is a term of the extended Boussinesq approximation that accounts for temporal changes in concentration and/or temperature and variation in density in directions orthogonal to the direction of flow. The representative equation for mass transport is given as (Diersch, 1998)

$$R_d \frac{\partial C}{\partial t} + q \cdot \nabla C - \nabla \cdot (D \cdot \nabla C) + Q_p C = Q_C \qquad (2.8)$$

where R_d is a derivation term of retardation, D is the tensor of hydrodynamic dispersion, C is concentration, and Q_C is the source/sink function of mass. The representative equation for heat transport is given as (Diersch, 1998)

$$[\theta \rho c + (1 - \theta)\rho_s c_s] \frac{\partial T}{\partial t} + \rho c q \cdot \nabla T - \nabla(\lambda_s \cdot \nabla T) + \rho c Q_\rho (T - T_0) = Q_T \qquad (2.9)$$

where θ is porosity, ρ_s is density of the solid phase, c_s is specific heat capacity of the solid phase, T is temperature, λ_s is thermal conductivity of solid phase, T_0 is a reference temperature, and Q_T is the source/sink function of heat.

2.4 Flow Model Calibration

The objective of the calibration process is to select the base-case, uniform (no spatial variability) flow and saltwater intrusion parameters that yield a modeling result as close to reality (if known) as possible. The idea then is to individually quantify the impact of the uncertainty of these parameters and other transport parameters on the movement of radionuclides from the tests to the seafloor. The final result of this uncertainty analysis is a reduced set of uncertain flow and transport

parameters that significantly influence the transport results (travel times, location of the plume when it crosses the seafloor, etc.). The parameters with little effect (as compared to those with significant influence) will not be considered uncertain in the final stage of uncertainty analysis. In that stage, the values of the selected parameters are chosen at random from the generated distributions. The calibration is then an important step to identify the best estimate of the uncertain flow parameters, upon which all subsequent analysis is based.

Given the distance between the tests, each test site is modeled separately. The locations of the three model cross sections are presented in Figure 2.7. A finite-element mesh is generated for each model domain as shown in Figure 2.8. Finer resolution is needed in the transition zone region. Given that the transition zone can vary substantially in position as a result of different parameter values, the entire upper left-hand half of the domain is given the more detailed mesh. The model domains differ from one another in the topography of the land surface and bathymetry of the seafloor, each being specific for the given location. These differences are most clearly seen using vertical exaggeration (Figure 2.9).

2.4.1 Milrow Calibration and Base-case Parameters

Three sets of measured data are used to calibrate the flow model and select the base-case parameters. Chloride concentration data at UAe-2 are used to identify the location and the width of the transition zone. Shallow head measurements that locate the water table from four wells are used
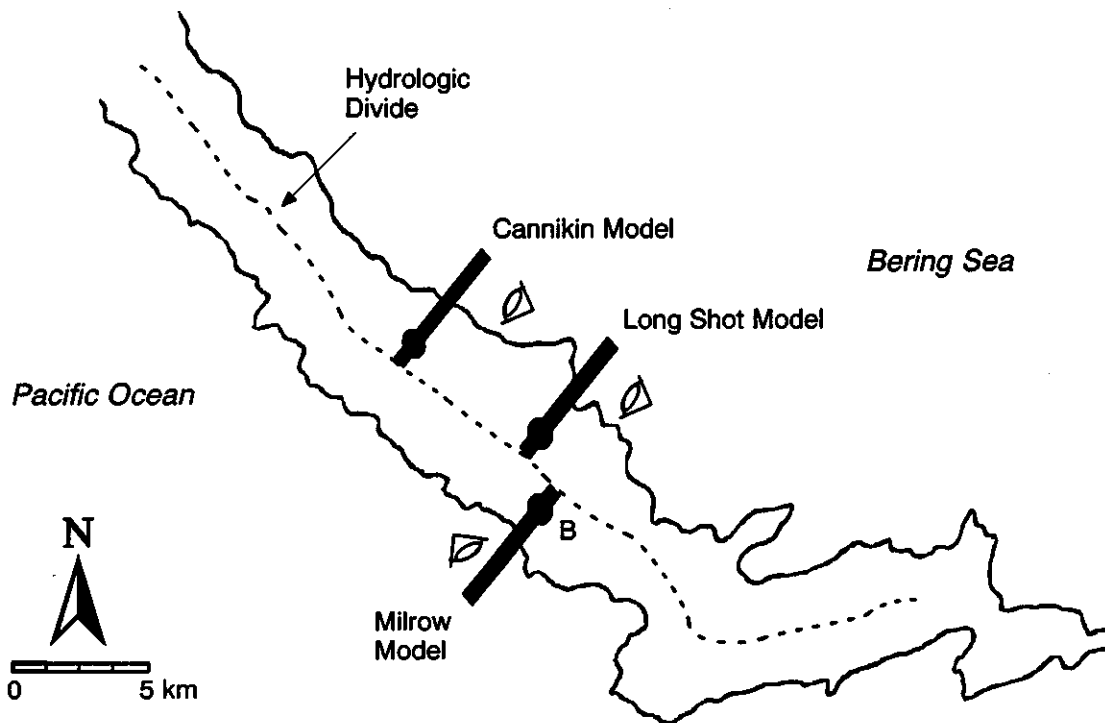

Figure 2.7. Location of model cross sections for each site. The cartoon eye shows the perspective of subsequent figures.
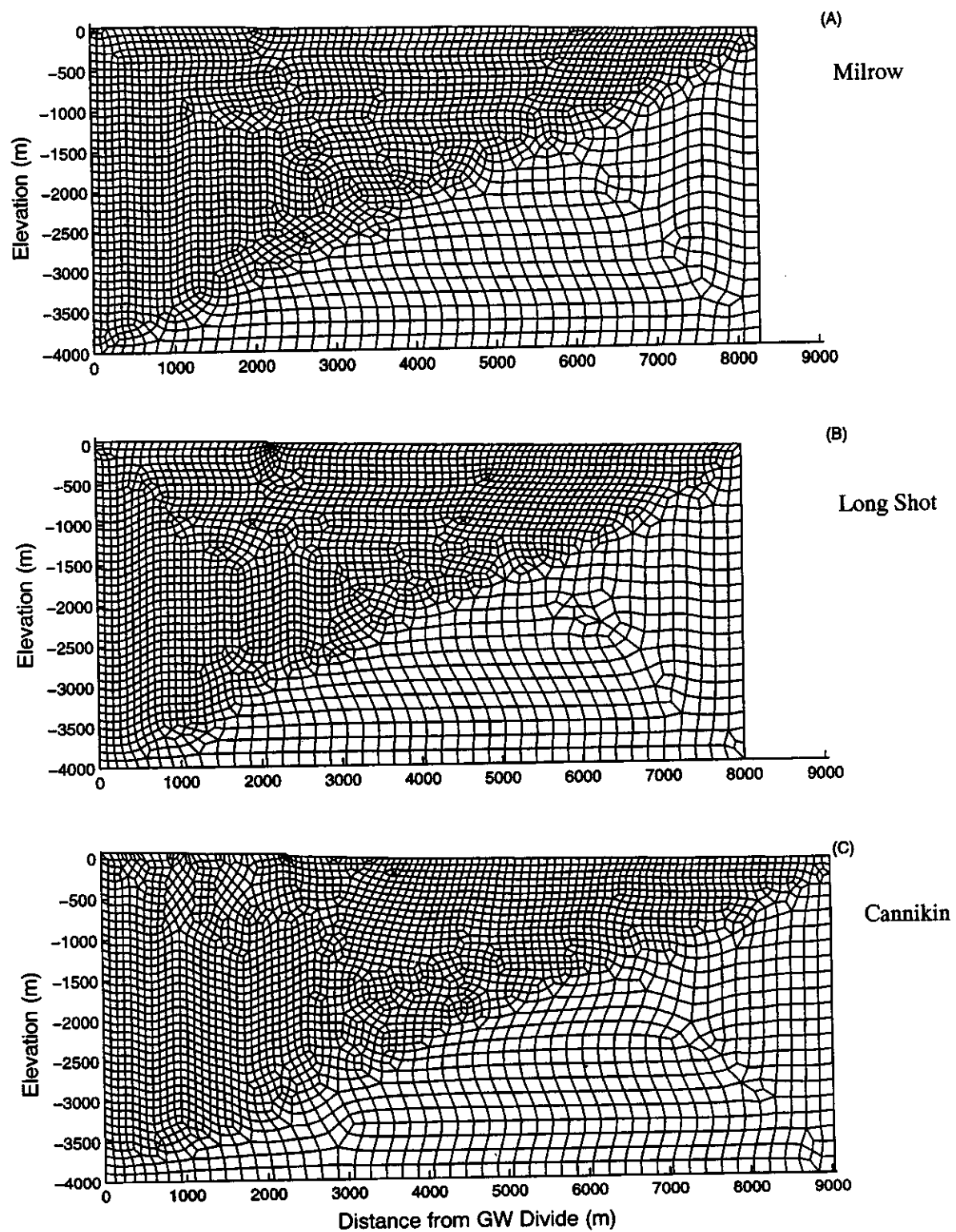
56

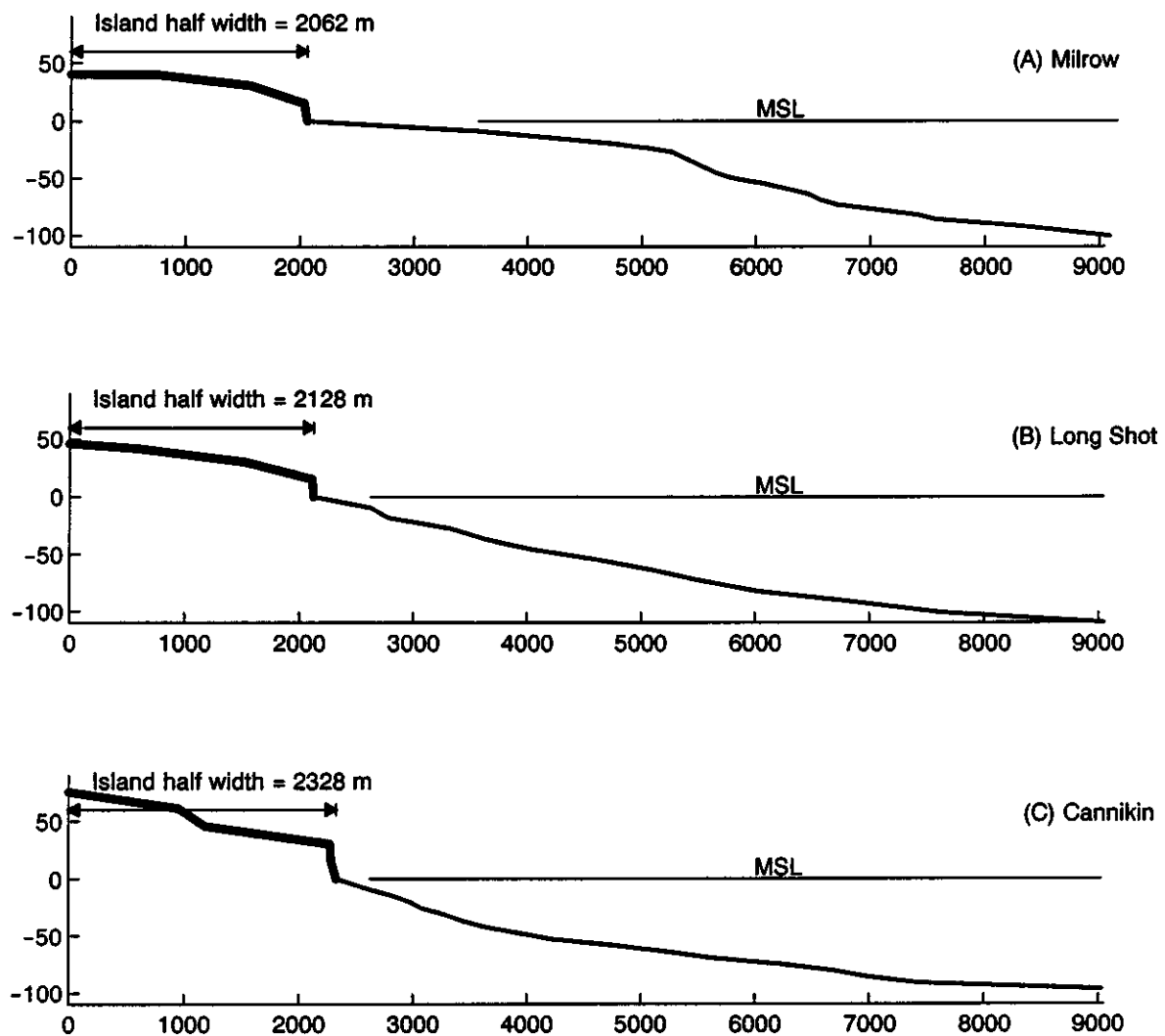**Figure 2.8.** Finite-element modeling meshes generated for each site model domain.

Figure 2.9. Topographic and bathymetric profiles used for each site-specific model. The diagrams use a tenfold vertical exaggeration.

as a second set of calibration data. The third set is the deep head measurements at UAe-2, which are used to compare with the modeled vertical head profile at the well location.

The geometry of the simulation domain and the boundary conditions are shown in Figure 2.10.

Recharge $C = C_f$

40

Specified Head

Island Center (GW Divide)

K_{zz}

K_{xx}

No-Flow
Boundary

$(P = \gamma h)$

$\partial C / \partial x = 0$

$C = C_s$

No-Flow Boundary $\partial C / \partial z = 0$
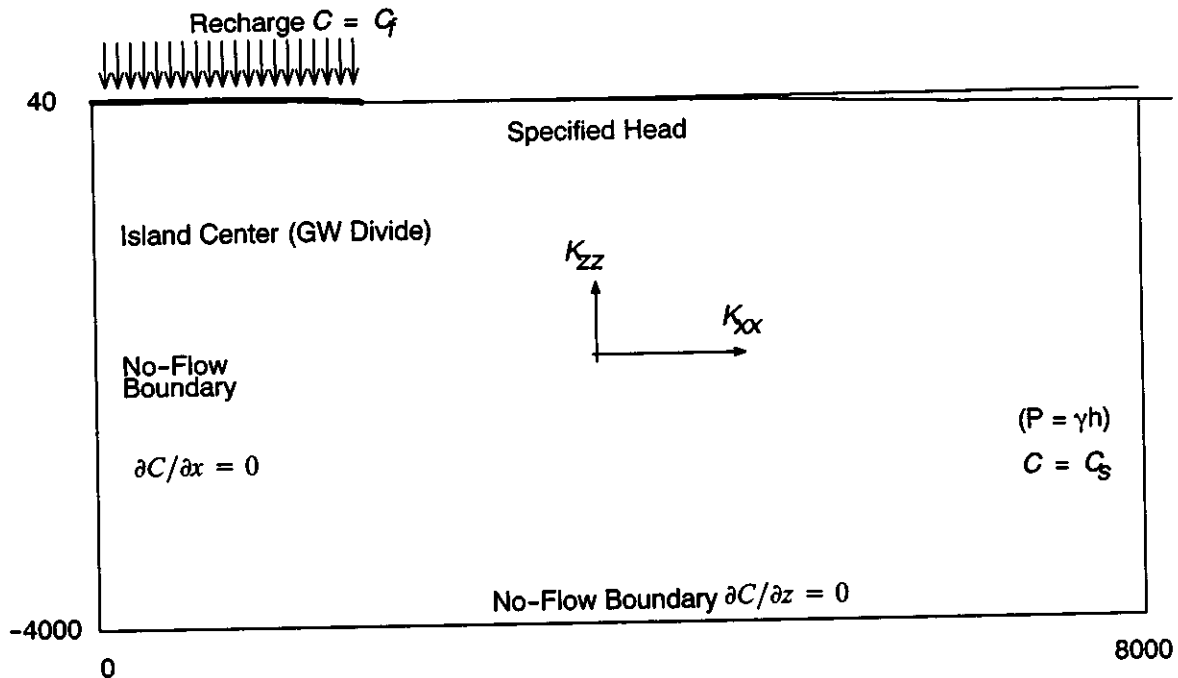
-4000

8000

0

Figure 2.10. Geometry of simulation domain and boundary conditions for the flow problem.

To allow for the sensitivity analysis of uncertain parameters, a domain length of 8,000 m is assumed, which is about four times the island half-width, and a thickness of 4,000 m is considered, which is more than three times the thickness of the freshwater lens (inferred from the Cl data at UAe-2) in the vertical direction. This provides the flexibility to change model parameters, and thus location and width of the transition zone, with no boundary effects influencing the resulting solution. The left-hand boundary is assumed to coincide with the groundwater divide at the island centerline, and as such, is assumed to be a no-flow boundary. The bottom boundary is also assumed to be a no-flow boundary. The right-hand boundary is a specified head and a constant concentration boundary. The top boundary is divided into two segments: a freshwater recharge segment representing the island half-width, and a specified head segment representing the seafloor (bathymetric profile). The bathymetric profile is best seen using vertical exaggeration as on Figure 2.9.

The two-dimensional domain is considered to be anisotropic ($K_{xx} \neq K_{zz}$) with anisotropy ratio $e = K_{xx}/K_{zz}$, and homogeneous (no spatial variability). Spatial variability only appears when accounting for the chimney porosity and permeability relative to the surrounding area. However, since calibration data are based on pre-test conditions, uniform conductivity and porosity throughout the domain is assumed at this stage. In a typical groundwater flow system, the spatial variability of hydraulic conductivity leads to a heterogeneous velocity field that exhibits variations at all scales of observation. This randomly changing velocity between blocks of varying conductivity induces an additional mixing process that is usually denoted as dispersion. This large-scale dispersive process can be substituted by

59

a macrodispersivity value in a homogeneous conductivity setting. This assumes that dispersion can be considered Fickian and macrodispersivities can be used to mimic the dispersive process caused by spatial variability (*e.g.*, Gelhar and Axness, 1983; Hess *et al.*, 1992). For this reason and for computational convenience, a homogeneous domain with anisotropic conductivity values is assumed. This is also justified by the fact that the density-driven flow pattern is very heterogeneous and adding spatial variabilities in hydraulic conductivity may only slightly change the flow pattern at and near the transition zone, which is the zone of importance for transport modeling. In addition, with hydraulic conductivity data from six wells spaced many kilometers apart on the island, the data abundance and locations will not support analysis of spatial correlations.

A large number of scenarios have been tested using FEFLOW, in which the homogeneous hydraulic conductivity and its anisotropy ratio, the recharge and the macrodispersivity are varied and the results are evaluated and compared to the calibration data. Table 2.4 lists the parameters used in all FEFLOW simulations presented in this study. Porosity does not affect the head distribution nor the location and width of the transition zone; it just speeds up or slows down the convergence of the system to the steady state. The macrodispersivity values are taken as 350 m and 175 m in the longitudinal and transverse directions, respectively. These values are chosen very large in an attempt to reproduce the transition-zone dispersion pattern indicated by the chloride data. The initial values of conductivity and recharge are selected based on the analysis of the available data and the variability observed therein, as discussed in Sections 2.2.1 and 2.2.4. The values are then changed based on the behavior of the simulated transition zone and heads in comparison with the measurements. Figure 2.11 shows an example of the FEFLOW output solutions in terms of concentration distribution and transition zone location (top) and velocity field (bottom). From the results of these tests, a single set of parameters to give a good match with all calibration data (shallow and deep heads and concentration data) could not be identified. Some of these cases are shown in Figure 2.12 for the comparison between the simulated and the measured heads. The simulated heads are obtained as freshwater equivalents or as environmental heads. The former is the direct output of FEFLOW, whereas the latter utilizes the actual specific weight that is dependent on the concentration. The measured head values should represent the environmental head provided no dilution occurs during the measurement process.

Table 2.4.   Parameters used in FEFLOW to solve the isothermal density-driven flow problem.

Parameter	Value
Freshwater density (kg_{water}/m^3)	1,000
Saltwater density (kg_{water}/m^3)	1,025
Freshwater concentration (C/C_{max})	2.67×10^{-3}
Seawater concentration (C/C_{max})	1.0
Density ratio	0.025
Diffusivity of solute in fluid (m^2/d)	8.88×10^{-9}
Specific storage, Ss	1.0×10^{-4}

The concentration distribution in UAe-2 is also compared to the FEFLOW results for the cases considered (the comparison is not shown). Concentrations were measured in water swabbed from
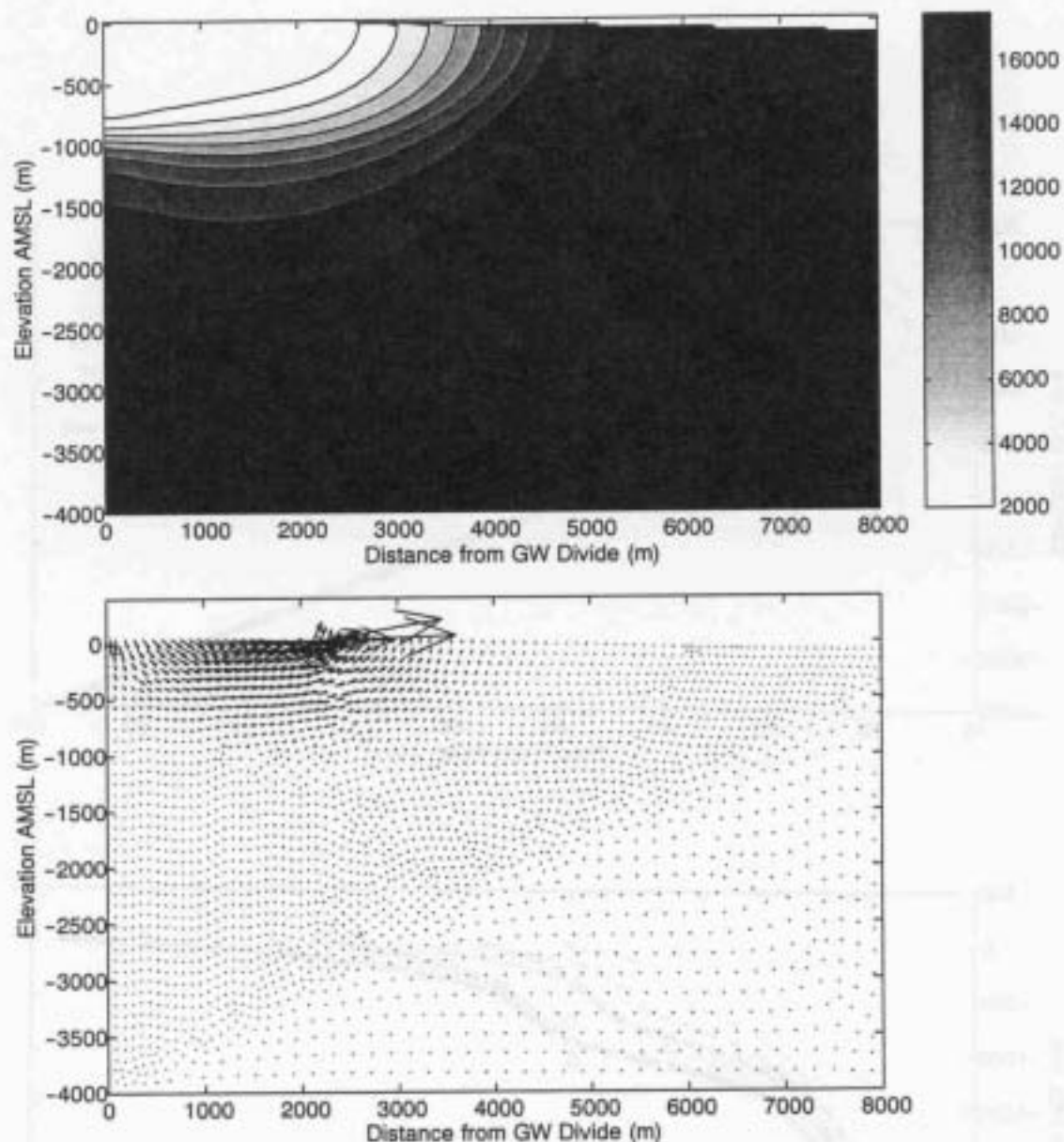
60

Figure 2.11. Concentration distribution showing transition zone (top) and velocity field as produced by
FEFLOW for one of the Milrow calibration cases tested.

60-m packer intervals during hydraulic testing and therefore represent composite values for the
entire corresponding intervals, and may also reflect mixing with borehole water originating from
other intervals. The comparisons indicate that a certain combination of the input parameters yields
a general agreement between simulated and measured concentration data, but simulates head values
smaller than measured. The results of this case are shown in Figure 2.13 and Figure 2.14. On the
other hand, Figure 2.15 and Figure 2.16 show very good match for the head, both deep and shallow,
but result in a thicker freshwater lens than what is indicated by the concentration data. To reduce this
thickness, a smaller recharge (or larger conductivity) value is needed, but this results in lower
simulated heads than measured. Changing the anisotropy ratio, e, plays a role as shown in
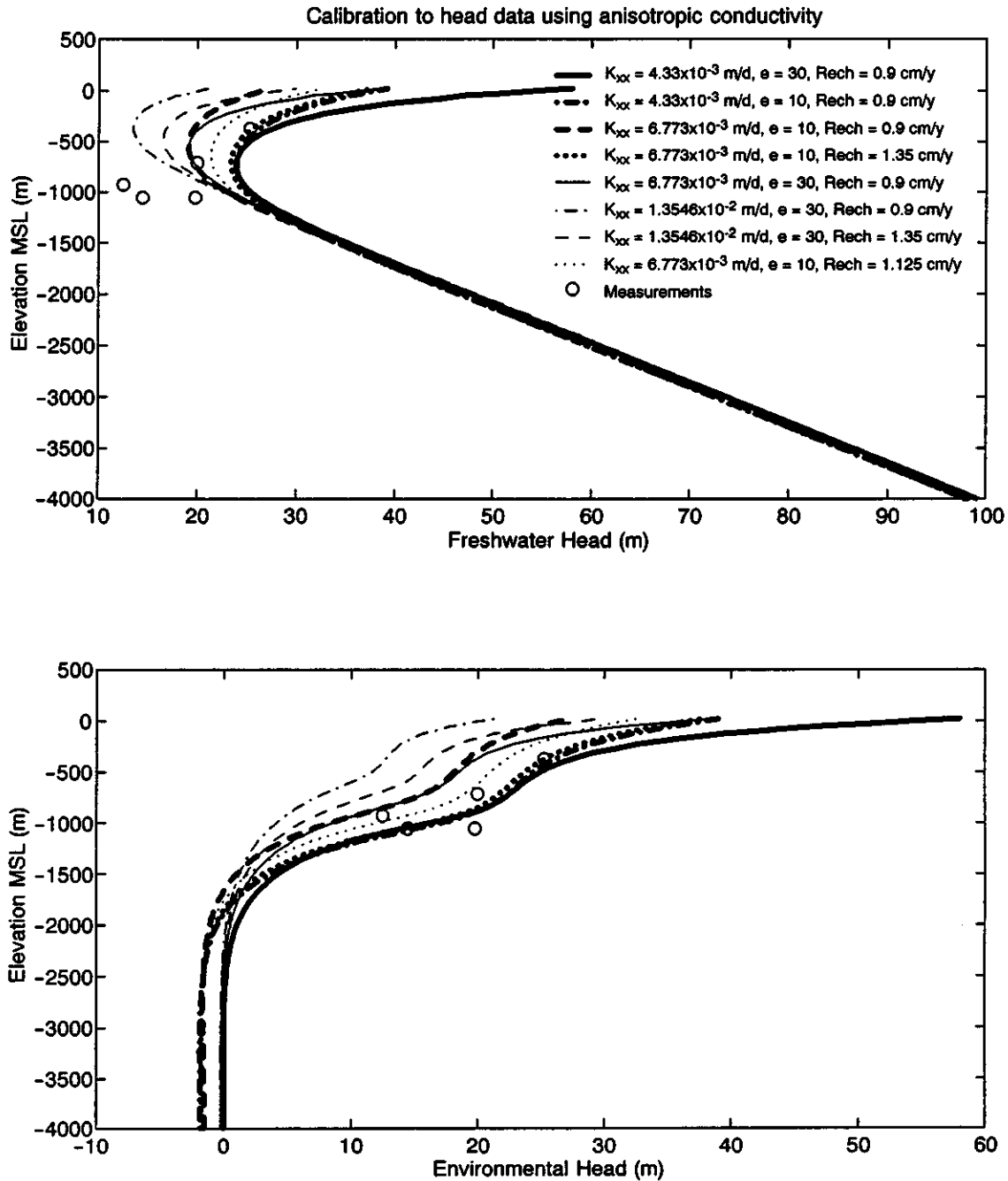
61

Figure 2.12. Comparison between simulated and measured heads for eight cases of different conductivity, anisotropy ratio and recharge combinations for Milrow.
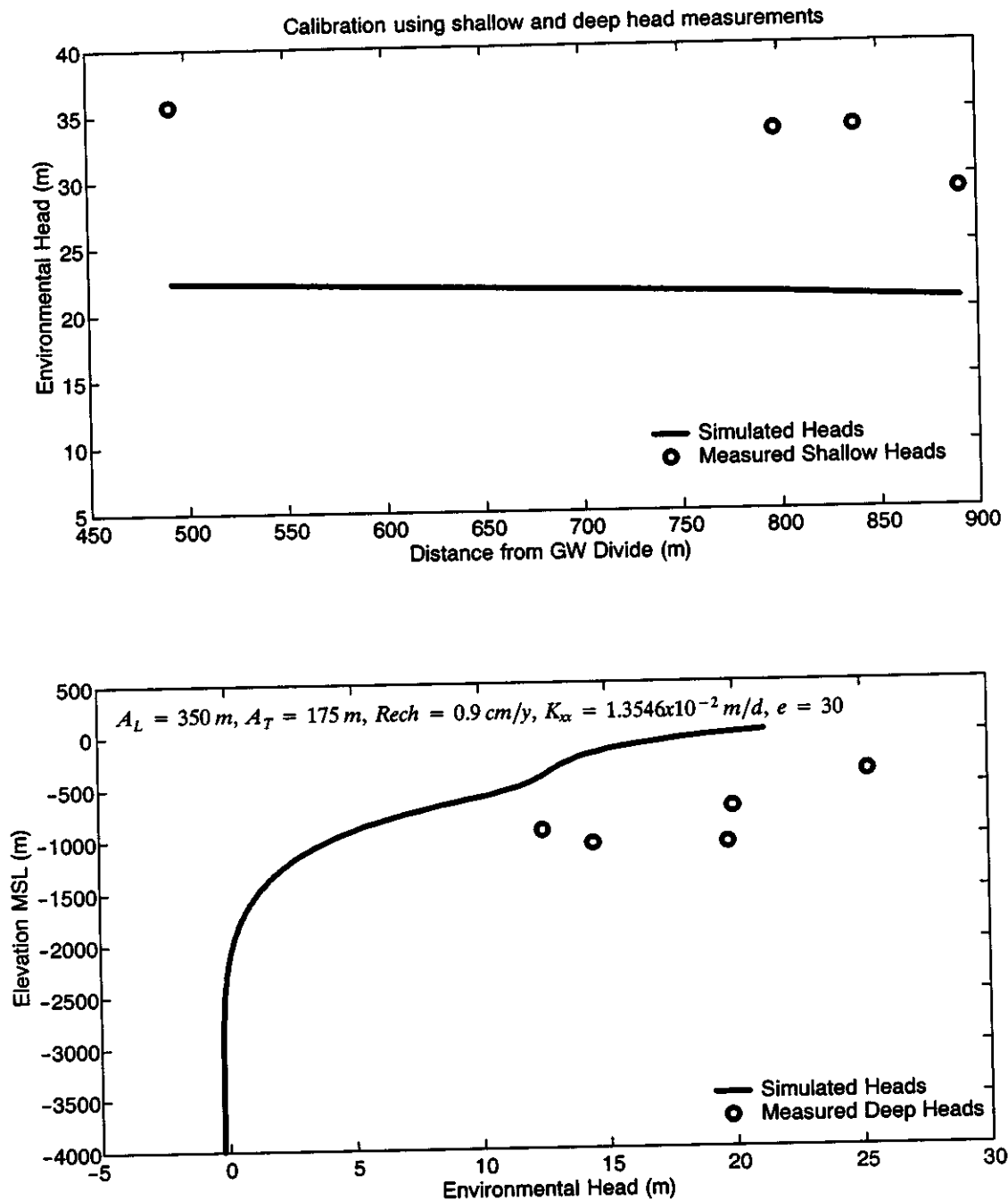
Calibration using shallow and deep head measurements

Environmental Head (m)

Distance from GW Divide (m)

— Simulated Heads
O Measured Shallow Heads

$A_L = 350\,m,\ A_T = 175\,m,\ Rech = 0.9\,cm/y,\ K_{xx} = 1.3546x10^{-2}\,m/d,\ e = 30$

Elevation MSL (m)

Environmental Head (m)

— Simulated Heads
O Measured Deep Heads

Figure 2.13. Comparison between simulated and measured heads for a Milrow case that leads to a good match for concentrations only.

Calibration with anisotropic conductivity, K_{xx}, $= 1.356 \times 10^{-2}$ m/d, $e = 30$

$A_L = 350\,m$, $A_T = 175\,m$, $Rech = 0.9\,cm/y$
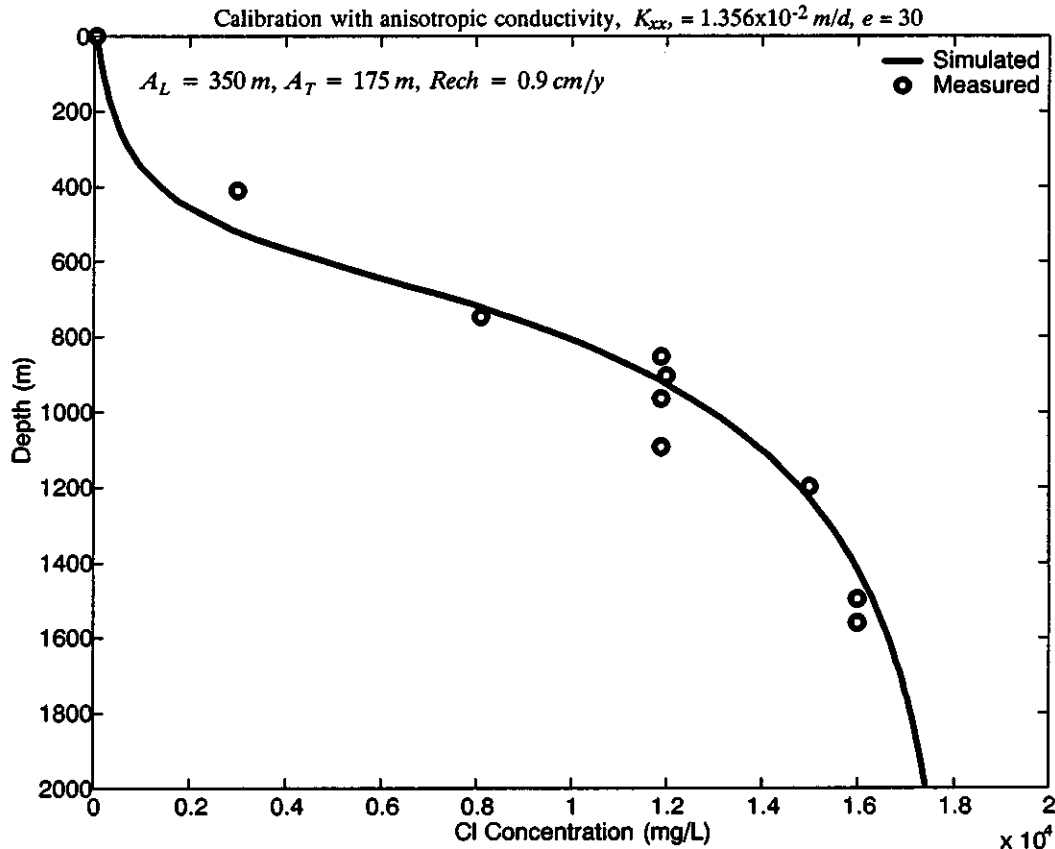
— Simulated
○ Measured

Figure 2.14. Comparison between simulated and measured chloride concentrations for a case that gives the best match to Milrow concentration data.

Figure 2.12, but a parameter combination that would result in matching all the measurements available for calibration could not be identified.

Since the objective of this calibration stage is to select the "mean" values of the parameters of concern, and since the uncertainty analysis will vary these parameters around the "mean" value, it is not crucial to match all the given calibration data. The uncertainty analysis will most likely cover the range of variability that is encountered in the plots of Figure 2.12. That is to say, any one of the combinations shown in Figure 2.12 will definitely be considered in the range of parameters employed for the uncertainty analysis discussed in Section 4. Therefore, the case shown in Figure 2.15 and Figure 2.17represents the base-case scenario, and the parameter values represent the mean values around which the random distributions will be generated. There are two reasons governing the choice of this case (better match of heads) as opposed to the other case where concentration data match better. First, since the concentration data may be affected by temporal changes in seawater level and/or the recharge amount, they may represent a thicker transition zone than represented by the steady-state result of the model. If the transition zone is moving vertically due to these changes, an additional spreading of saltwater will occur, leading to this thick transition zone. Secondly, changing the values of longitudinal and transverse macrodispersivities from 350 and 175 m to 100 and 10 m resulted in a transition zone depth (distance from ground surface to the 50% seawater concentration) close to what is indicated by the concentration data but with a smaller
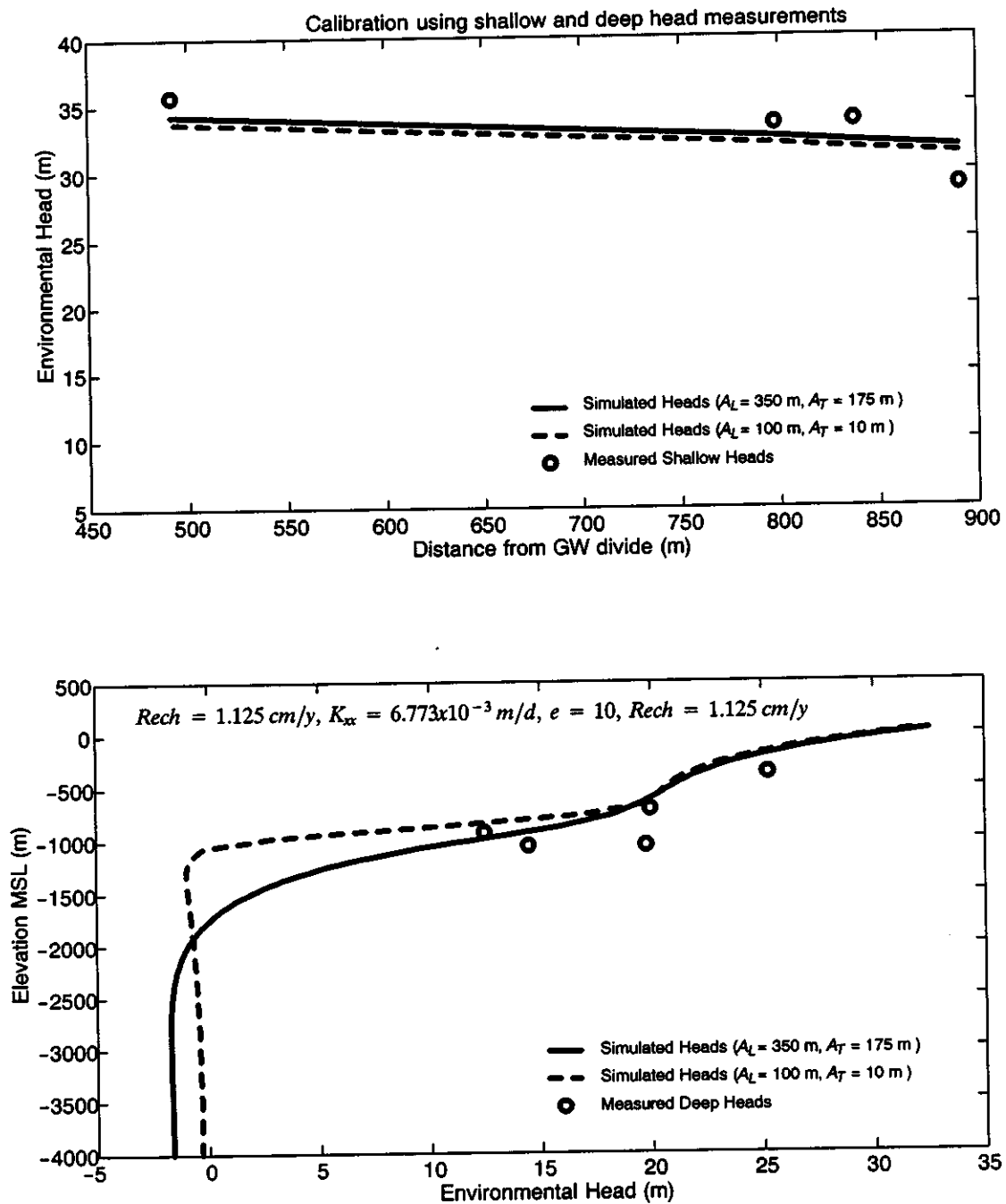
64

Calibration using shallow and deep head measurements

(top figure) — Simulated Heads (A_L = 350 m, A_T = 175 m); Simulated Heads (A_L = 100 m, A_T = 10 m); ○ Measured Shallow Heads

Axis labels: Environmental Head (m) vs. Distance from GW divide (m)

(bottom figure) — $Rech$ = 1.125 cm/y, K_{xx} = 6.773x10^{-3} m/d, e = 10, $Rech$ = 1.125 cm/y

Simulated Heads (A_L = 350 m, A_T = 175 m); Simulated Heads (A_L = 100 m, A_T = 10 m); ○ Measured Deep Heads

Axis labels: Elevation MSL (m) vs. Environmental Head (m)

Figure 2.15. Comparison between simulated and measured heads for a case that leads to a good match for Milrow heads only.
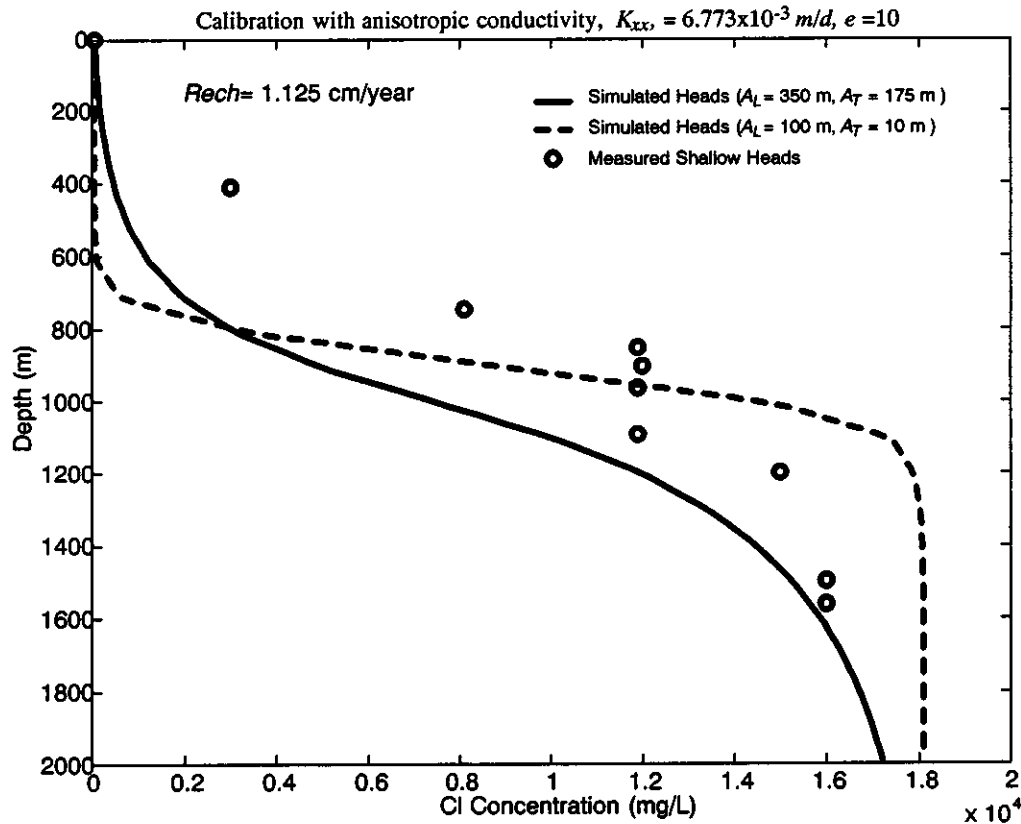
Figure 2.16. Comparison between simulated and measured chloride concentrations at Milrow for two cases of macrodispersivity. The larger values (350 and 175 m) yield a deep freshwater lens and thick transition zone; the smaller values (100 and 10 m) give a shallower lens and sharper transition from freshwater to seawater concentrations.

thickness (Figure 2.14) and still achieved good match with shallow and deep head measurements (Figure 2.13).

2.4.2 Long Shot Calibration and Base-case Parameters

Head data are available at a number of wells located within 100 m from the working point of Long Shot. Chloride concentration data are estimated from fluid concentrations at EH-5. The data are clustered in a small area around the cavity in such a way that the data points could be compared to a vertical head profile through the ground zero location. The concentration data points are clustered between 400 and 700 m below ground surface with chloride concentrations below 500 mg/L. These data cannot be used to identify the location and/or depth of the transition zone, but at least can be used as a guide to control the choice of model parameters.

The geometry of the simulation domain and the boundary conditions are similar to Milrow. The only difference is the shape of the upper boundary, which is determined by the topographic and bathymetric profiles (Figure 2.9). The island half-width is about 2,128 m for Long Shot, which is about 66 m wider than that of Milrow. The finite-element mesh used to discretize the simulation domain is similar to the other two tests.
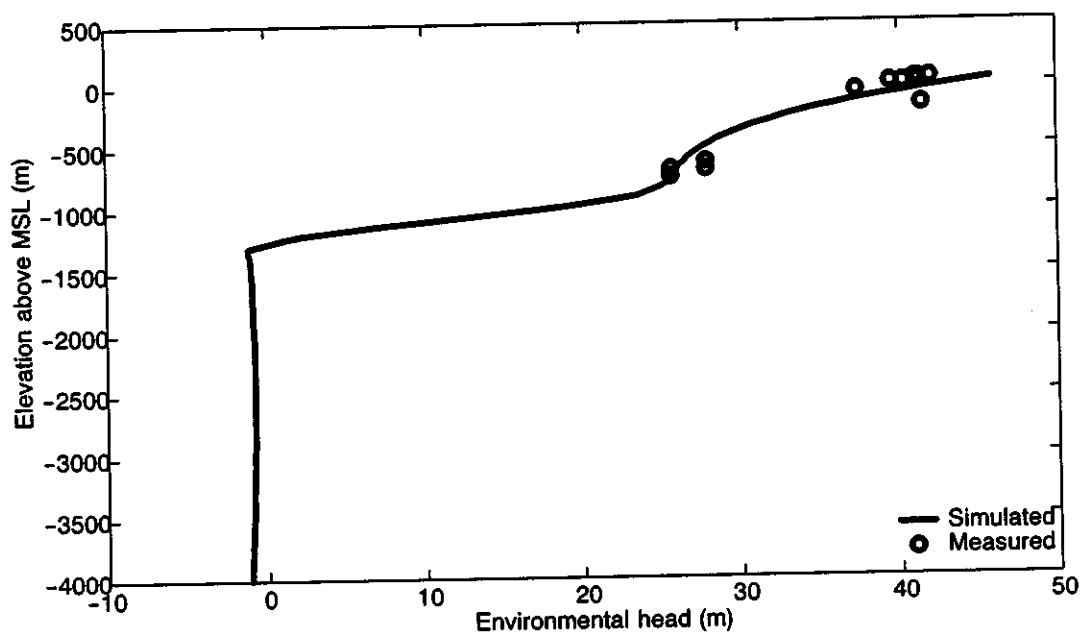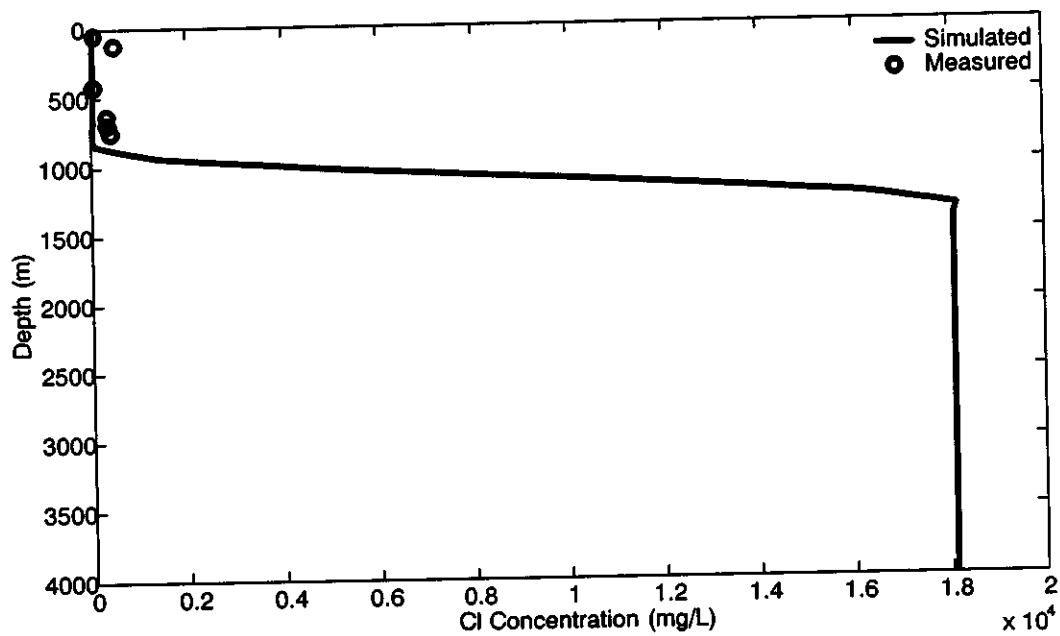
Figure 2.17. Long Shot calibration using concentration data at one well and head data at a number of wells clustered around the working point.

A number of parameter combinations have been tested, as was done for Milrow, and the response of the model was compared to available head and concentration data. The higher heads at EH-5 as compared to UAe-2 of Milrow indicate that a larger recharge-conductivity ratio is needed for the Long Shot model to match the data. Based on this difference and after running a number of simulations, the Long Shot calibration resulted in a recharge value of 3.65 cm/year and a conductivity value of 1.58×10^{-2} m/d, and thus the recharge-conductivity ratio for this calibration is about 6.3×10^{-3}.

Figure 2.17 depicts the comparison between concentration and head data and the simulation results. The concentration data do not provide sufficient information to delineate the transition zone location. The simulated concentration distribution at the EH-5 location is well matched, though slightly underestimating some of the measured concentrations. The simulated head profile also closely matches all the data points collected at different depths from different wells. Since these wells are located within one mesh element, and the variations of heads between adjacent elements occur slowly in the horizontal direction, comparing these head data to a vertical profile at a single location is considered reasonable.

2.4.3 Cannikin Calibration and Base-case Parameters

Two sets of measured data are available to calibrate the flow model and select the base-case parameters for Cannikin. Chloride concentration data at UAe-1 are used to help identify the location and the width of the transition zone. However, the data are clustered between 1,600 m and 2,000 m below ground surface with concentrations below 2,000 mg/L. These data cannot be used to identify the location and/or depth of the transition zone, but at least can be used as a guide to control the choice of model parameters. On the other hand, head measurements are available for three wells, UAe-1, UA-1, and HTH-1, which can be used to compare with the modeled vertical head profiles at the wells' locations.

The geometry of the simulation domain and the boundary conditions are not different from the other sites and are as shown in Figure 2.10. The only difference is the shape of the upper boundary, which is determined by the topographic and bathymetric profiles (Figure 2.9). These profiles for Cannikin are different from those for Milrow and Long Shot. For example, the island half-width is about 2,328 m for Cannikin, whereas Milrow and Long Shot have an island half-width of about 2,062 and 2,128 m, respectively. The two-dimensional domain is discretized in a manner similar to Milrow, where the upper left half is assigned a mesh size of 100 m and the other half is assigned a mesh size of 200 m.

A large number of scenarios have been tested using FEFLOW, in which the homogeneous hydraulic conductivity and its anisotropy ratio, the recharge and the macrodispersivity are varied and the results are evaluated and compared to the calibration data. The macrodispersivity values are taken as 100 m and 10 m in the longitudinal and transverse directions, respectively. The value of porosity is not important at this stage, as the domain is assigned a uniform porosity and chimney changes are not considered for the pre-test calibration conditions. The initial values of conductivity and recharge are selected similar to those for the Milrow calibration. However, comparing the

chloride concentration data available for Cannikin and the head values at UAe-1 to those for Milrow and Long Shot indicates that a much deeper transition zone is more likely to be the case for Cannikin. After a number of trials, the values selected for the recharge and conductivity are higher than those for Milrow, and compared to Long Shot, the Cannikin conductivity is slightly lower and the recharge higher. The calibration resulted in a recharge value of 5.48 cm/year (as compared to 1.125 cm/year for Milrow and 3.65 cm/yr for Long Shot) and a conductivity value of 1.38×10^{-2} m/d (as compared to 6.677×10^{-3} m/d for Milrow and 1.58×10^{-2} m/d for Long Shot). This resulted in a recharge-conductivity ratio of 1.09×10^{-2} as opposed to 4.62×10^{-3} for Milrow and 6.3×10^{-3} for Long Shot, and as such, a deeper transition zone is obtained.

The transition zone is not the only factor controlling the choice of the calibration parameters. The head measurements in the three wells, although not always useful, provide another criterion for calibrating the flow model. In general, the head data for Cannikin wells indicate higher heads than observed at Milrow. To reproduce these higher heads, a higher recharge value is necessary as compared to Milrow. Figure 2.18 shows the comparison between the measurements and the modeling results for the concentration and head data at UAe-1. The concentration profile does not match the data collected below a depth of 1500 m. The head comparison for UAe-1 shows that the simulated heads pass through the range of the measurements, which do not provide a clear vertical head profile. Figure 2.19 shows the head comparisons for UA-1 and HTH-1. Simulated heads are matching closely the measured heads for UA-1, although positive and negative deviations exist. On the other hand, simulated heads are higher than measured for HTH-1. The two calibration figures indicate that simulations result in a compromise in terms of matching the heads at UAe-1, UA-1, and HTH-1. That is, any increase in the recharge-conductivity ratio will not improve the match for UAe-1, but will increase the existing deviations for HTH-1. Decreasing this ratio, on the other hand, may improve the comparison for HTH-1, but will cause larger head deviations for both UAe-1 and UA-1 and larger concentration deviations for UAe-1. Considering the fact that the quality of the concentration data at UAe-1 has been a source of suspicion in many studies, and the possible violation of the steady state assumption for the chemistry profile, compromising in terms of matching the head data at the three wells is regarded as a reasonable calibration result. In addition, the final modeling stage encounters many realizations that provide a wide range of scenarios and results that encompass most of the data available from the three wells.

2.4.4 Summary of Calibration Results

The final calibration values are summarized in Table 2.5 and the corresponding transition zones can be seen on Figure 2.20. The lower recharge-conductivity ratio at Milrow results in a shallower transition zone, consistent with the data. The slightly higher ratio for Long Shot increases the depth to the transition zone, and the much higher recharge-conductivity ratio for Cannikin extends its transition zone deeper still. Again, these different configurations for the freshwater-seawater system are consistent with the data for each site. There may be several contributing factors causing the variation in transition zone depth from one site to another. One contributor is topography, with the higher land elevation at Cannikin (23.5 m higher at the Cannikin emplacement well than at Milrow) resulting in a corresponding higher elevation of the water table, which is very near ground surface
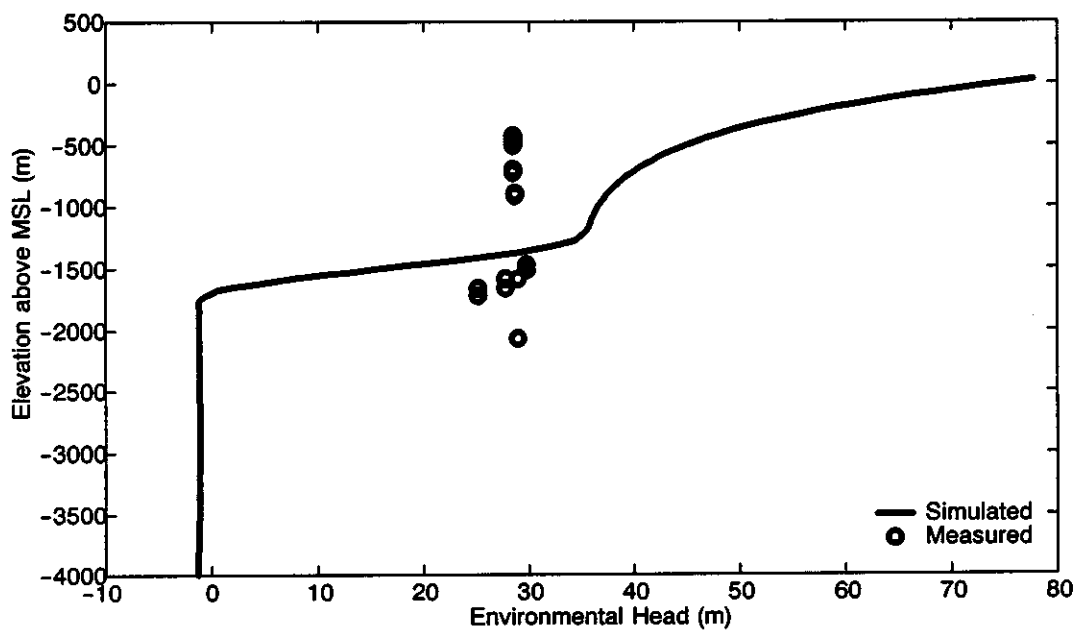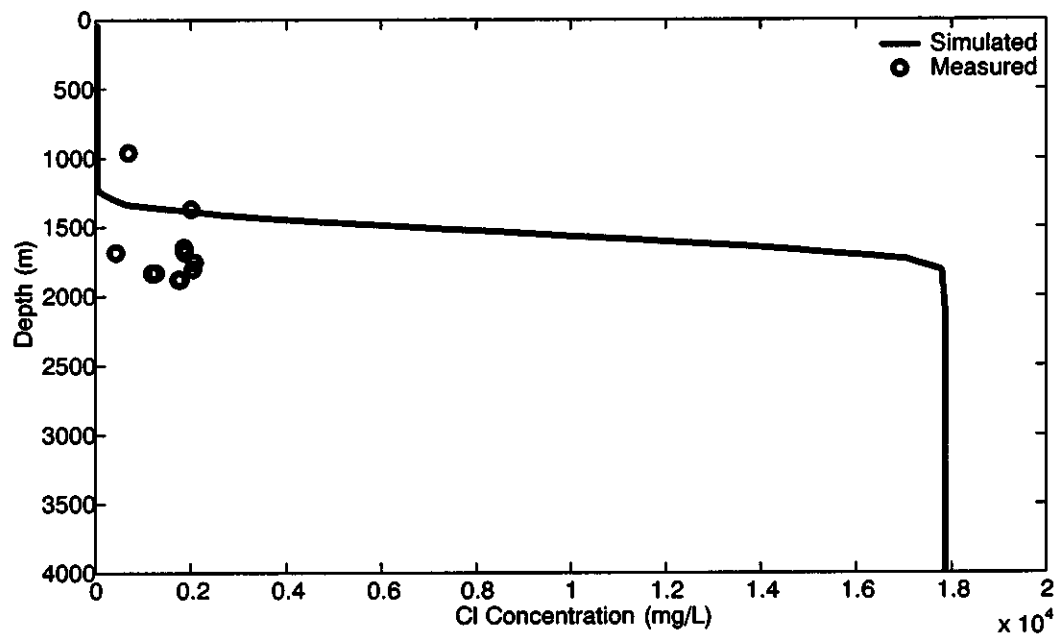
Figure 2.18. Calibration results for Cannikin well UAe-1 where head and concentration data are compared to model results.
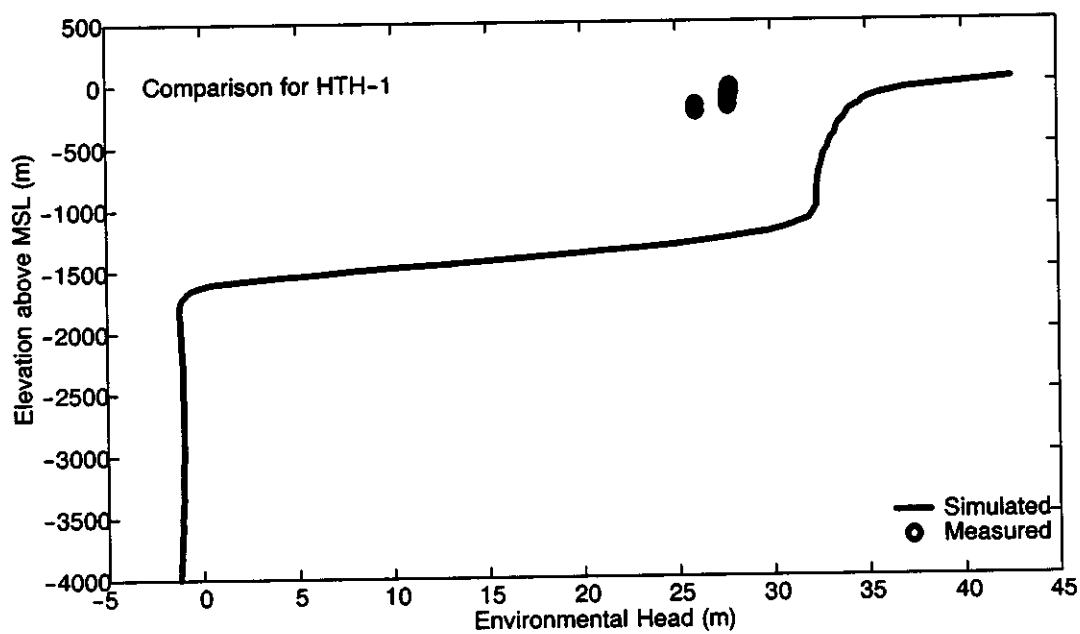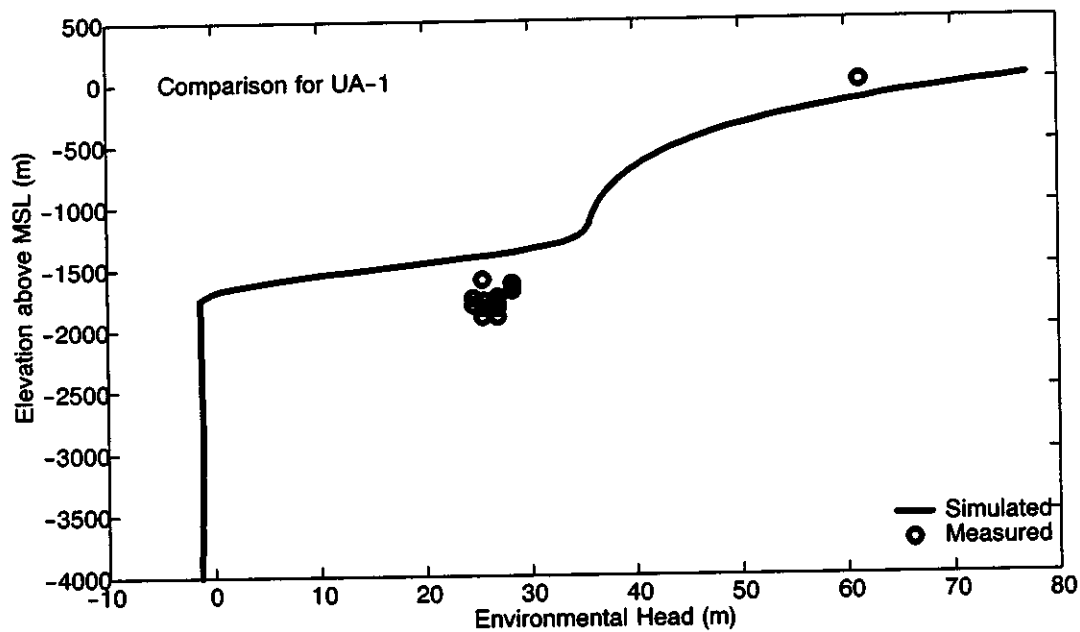
Figure 2.19. Calibration results for Cannikin wells UA-1 and HTH-1 using head data.
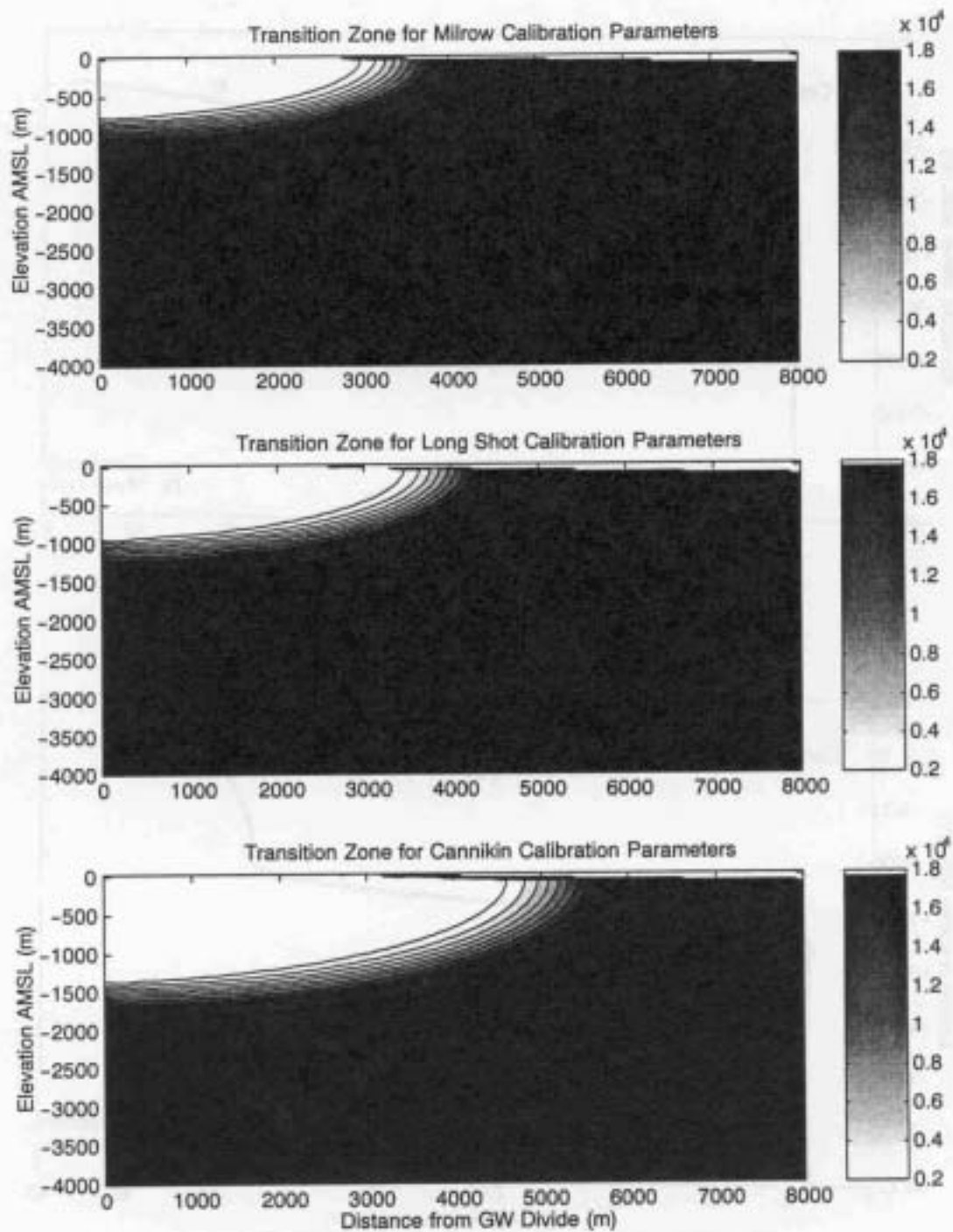
Figure 2.20. Transition zones modeled for each site using the calibration parameters, expressed by the chloride concentration.

at all locations. Another factor is the tendency toward higher hydraulic conductivity values at Cannikin for a given elevation relative to Milrow (data are presented in Section 2.2.1). Though the availability of recharge is not obviously different from one location to another, the ability of the subsurface to accept and transmit recharge is governed by the hydraulic conductivity.

Table 2.5.   Summary of calibration parameters.

Test	K (m/d)	Rech (cm/y)	K/Rech	A_L (m)	A_T (m)
Milrow	6.773×10^{-3}	1.125	4.62×10^{-3}	100	10
Long Shot	1.58×10^{-2}	3.65	6.3×10^{-3}	100	10
Cannikin	1.38×10^{-2}	5.48	1.09×10^{-2}	100	10

An asymmetry to the freshwater lens geometry has been suggested by other researchers, as well as the presence of a deeper freshwater lens at Cannikin (Fenske, 1972a; Dudley *et al.*, 1977). The impact of the transition zone on the groundwater velocity field for each site is shown in Figure 2.21. Given the very low velocities in the seawater portion of the domain, relatively high groundwater velocities at Milrow are confined to a much shallower region than at Long Shot and Cannikin with their deeper transition zones. Not only does the higher velocity transition zone extend deeper in the subsurface, but the reach of sea floor across which freshwater discharges is also extended farther out to sea. Thus, the freshwater lens simulated at Long Shot, and particularly Cannikin, is not only deeper but more laterally extensive than that simulated for Milrow.
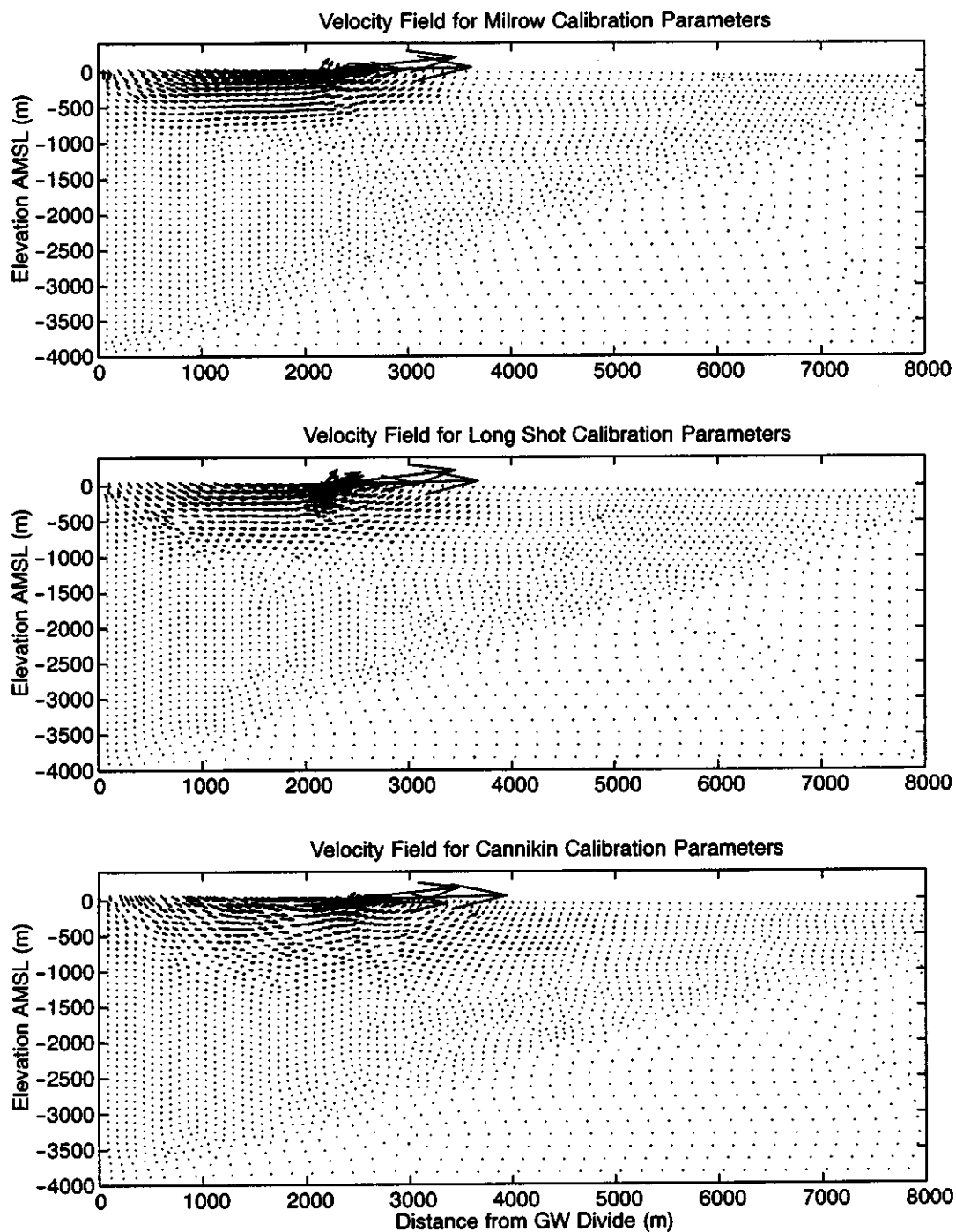
Figure 2.21. Velocity vectors for the calibrated flow fields at each site.